FOCUS ARTICLE

Guided selective deposition of nanoparticles by tuning of the surface potential

To cite this article: J. Eklöf *et al* 2017 *EPL* **119** 18004

A Letters Journal Exploring the Frontiers of Physics

July 2017

EPL, **119** (2017) 18004 www.epljournal.org
doi: 10.1209/0295-5075/119/18004

Focus Article

Guided selective deposition of nanoparticles by tuning of the surface potential[(a)]

J. Eklöf[1], A. Stolaś[1], M. Herzberg[2], A. Pekkari[1], B. Tebikachew[1], T. Gschneidtner[1], S. Lara-Avila[3], T. Hassenkam[2(b)] and K. Moth-Poulsen[1(c)]

[1] *Department of Chemistry and Chemical Engineering, Chalmers University of Technology Gothenburg 412 96, Sweden*
[2] *Nano-Science Center, Department of Chemistry , University of Copenhagen - Universitetsparken 5, 2100, Copenhagen, Denmark*
[3] *Department of Microtechnology and Nanoscience, Chalmers University of Technology Gothenburg 412 96, Sweden*

received 7 June 2017; accepted 31 August 2017
published online 19 September 2017

PACS 82.20.Kh – Potential energy surfaces for chemical reactions
PACS 83.80.Hj – Suspensions, dispersions, pastes, slurries, colloids

Abstract – Guided deposition of nanoparticles onto different substrates is of great importance for a variety of applications such as biosensing, targeted cancer therapy, anti-bacterial coatings and single molecular electronics. It is therefore important to gain an understanding of what parameters are involved in the deposition of nanoparticles. In this work we have deposited 60 nm, negatively charged, citrate stabilized gold nanoparticles onto microstructures consisting of six different materials, (vanadium (V), silicon dioxide (SiO_2), gold (Au), aluminum (Al), copper (Cu) and nickel (Ni)). The samples have then been investigated by scanning electron microscopy to extract the particle density. The surface potential was calculated from the measured surface charge density maps measured by atomic force microscopy while the samples were submerged in a KCl water solution. These values were compared with literature values of the isoelectric points (IEP) of different oxides formed on the metals in an ambient environment. According to measurements, Al had the highest surface potential followed by Ni and Cu. The same trend was observed for the nanoparticle densities. No particles were found on V, SiO_2 and Au. The literature values of the IEP showed a different trend compared to the surface potential measurements concluding that IEP is not a reliable parameter for the prediction of NP deposition.

Introduction. – Nanoparticles (NP) have attracted broad interest during recent decades due to their physical and chemical properties. Metal-oxide NPs efficiently protect against ultraviolet radiation [1] and silver (Ag) NPs are used in consumer products as anti-bacterial agents [2]. NPs can also be used in enhanced catalysis [3,4] in drug targeting for cancer therapy [5], breakdown of oil spillage [6], sensing applications [7–9] and as electrical contacts in the emergent field of single-molecule electronics [10–13]. The majority of these applications would benefit from a simple and controlled way of depositing NPs on surfaces in order to enable even more advanced functions [11]. It is therefore interesting to investigate how NPs can be guided onto different surfaces and to understand the parameters involved in this process, such as surface and particle potential.

There are already several techniques available today for the deposition of NPs onto surfaces. One way is to evaporate a thin film of metal onto a substrate. Particles will then start to form after annealing [14]. Another more refined way is to form a monodispersed NP-aerosol by heating a metal, sort the NPs of interest using a differential mobility analyzer and deposit them on a surface [15]. Electrospray deposition is another example where a dispersion of NPs is forced through a small nozzle and onto a substrate [16]. It has also been shown that it is possible to electrostatically deposit colloidal dispersions by applying a bias between an electrode and

[(a)] Contribution to the Focus Issue *Self-assemblies of Inorganic and Organic Nanomaterials* edited by Marie-Paule Pileni.
[(b)] E-mail: tue@nano.ku.dk
[(c)] E-mail: kasper.moth-poulsen@chalmers.se

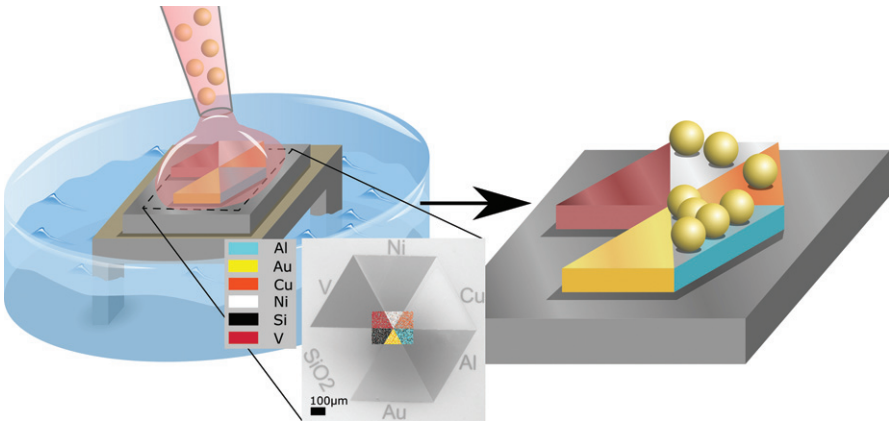

Fig. 1: (Colour online) Overview of the deposition procedure. Left: a drop of NPs is deposited onto a substrate of Si/SiO_2, with five different metals (V, Ni Cu, Al and Au) on. The substrate is placed onto a 3D printed scaffold placed in a beaker, with an attached lid. Water in the beaker prevents evaporation of the droplet during deposition. Right: the NPs are guided to selective areas of the substrate. A SEM image, including XEDS mapping over a hexagonal structure, confirming the elements can be seen in the middle.

the substrate [17]. There are examples where a surface is functionalized with molecules designed to attract NPs from a colloidal solution [11,18]. A drop of a NP dispersion is then applied onto the surface and the particles assembly onto the surface by themselves. Scientists have also developed ways to deposit particles by using capillary forces between a substrate and a glass slide. This creates a meniscus flow forcing the particles to assemble at the interface between substrate, dispersion and air [19,20].

In this work, we have focused on the deposition of colloidal citrate stabilized NPs dispersed in water. The particles are deposited onto different oxide and metal surfaces such as vanadium (V/V_2O_5), silicon dioxide (Si/SiO_2), gold (Au), aluminum (Al/Al_2O_3), copper (Cu/CuO) and nickel (Ni/NiO_2). The reason for choosing citrate stabilized NPs is due to their availability and broad use in many applications [8,9]. Due to the citrate ligand, further functionalization with functional molecules such as proteins are considered to be straightforward [21,22]. The metals above can with ease be evaporated onto a substrate forming any pattern of interest, which can be interesting for later applications where NPs are to be positioned at selected areas of a surface. It is known that Si forms a natural oxide SiO_2 [23] and Al forms Al_2O_3 [24]. The other metals, except for Au which is a noble metal, can form several types of oxides [25–27]. Multi-crystalline metal films were used in this work due to the evaporation step, which could lead to different types of oxides in ambient air. It could therefore be difficult to predict the exact surface charge from for example zero-point charge or tabulated values of the isoelectric point (IEP) [28,29], since the IEP changes between oxides of the same element. It was therefore necessary to investigate the local surface potential of the different surfaces in water, since the exact surface parameter is important [30], directly affecting the deposition of NPs. We investigated the correlation between the density of particles at the surface using scanning electron microscopy (SEM). The surface potential of the substrates was measured in water by measuring the surface charge density using an AFM (Asylum Research MFP-3D atomic force microscope) operating in 1 mM KCl dissolved in water. The surface charge densities were then used to calculate surface potentials (using the Grahame equation) [31]. The density of NPs at the different surfaces was calculated by letting an image processing software count NPs from micrographs of samples with NPs deposited on them. The samples consist of a Si/SiO_2 substrate with an array of five different metals (V, Au, Al, Cu, Ni) arranged in a hexagonal pattern (see fig. 1) all made using laser lithography.

Experimental. – Five different metals, V, Au, Al, Cu and Ni were evaporated to a thickness of 100 nm, in a specific pattern, fig. 1 onto a substrate of silicon(100) (Si) with thermally grown 280 nm thick silicon dioxide (SiO_2) (ordered from Si-mat). A 5 nm thick titanium film (Ti) was applied underneath the Au and Cu areas in order to improve adhesion to SiO_2.

Sample preparation. The following procedure was used to create each metal domain on the substrates. The substrate (Si/SiO_2) was cleaned with O_2-plasma (10 sccm, 250 mTorr, 50 W) for 1 min using a Dry etch RIE–PlasmaTherm–Oxygen. Subsequently, the substrate was covered with lift-off resist LOR 3A (supplier Microlithography Chemical Corp.) and spin-coated at 3000 rpm for 45 s, creating a film thickness of 0.36 μm. The substrate was then baked on a hotplate at 190 °C for 5 min and cleaned under a stream of N_2-gas. A second layer of photoresist S1813 (supplier Microresist GmBH) was applied on the substrate, it was then spin-coated at 3000 rpm for 45 s, creating a film thickness of 1.5 μm. The substrate was then baked at 100 °C and cleaned with N_2-gas. A laser writer DWL 2000, equipped with a 405 nm diode laser, was then used to expose the photoresist according to a pre-designed pattern. The substrate was then developed in MF319 for 45 s, rinsed with deionized water and blow

dried with N_2-gas. The sample was cleaned in 1 min of O_2 plasma (10 sccm, 250 mTorr, 50 W) before a metal film was evaporated ontop of the double layer resist using a Lesker PVD 255 Evaporator system. 5 nm Ti was evaporated before evaporating Cu or Au for improved adhesion. The lift-off was performed in an ultrasonic bath filled with mr-Rem 400 heated to 50 °C during 30 min, followed by rinsing in a bath of filtered 2-propanol, deionized water and finally dried with N_2-gas. This procedure was repeated for each metal.

Deposition. In this work, 60 nm spherical Au NPs, stabilized in trisodium citrate, were supplied from Sigma Aldrich (prod. No. 742015) as a colloidal dispersion. A plastic vial (Eppendorf 3810X 1.5 mL) was filled with 1 mL of the dispersion and centrifuged for 10 min at 2400 g, in order to force the NPs to the bottom of the vial. The supernatant fluid was removed, 1 mL of deionized water was added to the vial and the NPs were dispersed in the fluid. The vial was then centrifuged a second time (10 min, 2400 g) and the supernatant was removed leaving 0.5 mL residual dispersion. The NPs were then re-dispersed, and a drop was added onto the sample. A scaffold system with controlled atmosphere (fig. 1) [18] was used for the substrate during the deposition, preventing the droplet to dry out during the deposition. The remaining dispersion was rinsed away, after the deposition (60 min), in a beaker of deionized water and dried with N_2-gas.

TEM, SEM and XEDS. The size of the NPs was inspected using a TEM, Tecnai T20 microscope, operating at 200 kV with a LaB6 filament. 5 μL of the NP dispersion (prepared in the same way as the one used for deposition) was dropped on TEM grid (carbon support film, 200 Mesh 3 mm copper grid) and left to dry for 3 hours.

The samples were investigated using the In-Lens detector of a Zeiss Supra 60 VP SEM operating at 12 kV (at a pressure of $7 \cdot 10^{-7}$ mbar using the 30 μm aperture). The images were then later analyzed using an image processing software [18]. The nanoparticle surface density was calculated by dividing the number of particles found in the image with the image size.

The metals and semiconductor materials used to build the hexagonal structures were confirmed by an X-ray energy dispersive spectroscopy (XEDS) from Oxford Inca EDS/EDX systems. A map of the results can be seen in fig. 1.

Zeta potential. The zeta potential of the NP dispersion was measured with Zeta Sizer Nano ZS instrument, model: ZEN 3600, Malvern Instruments, using folded capillary zeta cuvettes. The measurement was recorded in three series, each contained 50 runs.

AFM. Force maps were achieved using Asylum Research MFP-3D atomic force microscope (AFM). These maps were used to reconstruct surface charge density maps by fitting force curves to DLVO theory [32–34].

The reconstruction method works by fitting an experimental force curve to a theoretical DLVO curve which is given by the following equation:

$$F = \int_0^\infty f_e \cdot 2\pi r \mathrm{d}r + \int_0^\infty f_{vdW} \cdot 2\pi r \mathrm{d}r, \tag{1}$$

where dr is the geometry of the tip described in [32]. The first term integrates the electrostatic force f_e,

$$f_e = \frac{2}{\epsilon_0 \epsilon_r} \left(\sigma_t \sigma_s e^{-\kappa D} + (\sigma_t^2 + \sigma_s^2) e^{-2\kappa D} \right), \tag{2}$$

where κ denotes the inverse debye length, [30] D the distance between the surface and the tip, σ_t is the known surface charge density of the tip, σ_s is the charge density of the substrate surface, ϵ_0 is the permittivity in vacuum, ϵ_r is set to 78, the permittivity of the water solution. The second term in eq. (1) integrates the van der Waals force, f_{vdW} (seen in the following equation), where A denotes the Hamaker constant [30],

$$f_{vdW} = -\frac{A}{6\pi D^3}. \tag{3}$$

The measurements were performed by gluing a chip to the sample holder with EPON Resin 1002F epoxy glue. An undecanethiol self-assembled monolayer (SAM) functionalized tip was then prepared in the following way: A biolever tip from Olympus Research with a spring constant of 34.12 pN/nm was cleaned with UV-generated ozone. The SAM on the tip was made by submerging the tip in a solution of 0.05 g undecanethiol in 50 mL 99.5% ethanol (5.5 mM) for 24 h [35]. This type of tip would make the contribution to the surface charge from the tip in eq. (2) neutral.

For the force measurements, a solution of KCl (1 mM) was prepared with reagent grade salt from Sigma Aldrich (99.5%) and pure deionized water (MilliQ, 18.2 M$\Omega \cdot$ cm). The resulting pH value was 5.49.

The sample holder was filled with 3 mL of 1 mM KCl solution and a 30×30 force map across an area of 5×5 μm was made for each of the six surfaces with a sample rate of 12.5 kHz. A force distance of 500 nm and a scan frequency of 1 Hz was used which resulted in a speed of 1000 nm/s. The indentation force was set to 500 pN, to ensure full contact to the surface before retracting the AFM tip.

The average surface charge density value was then extracted for each map and was used to calculate surface potential values with the Grahame equation,

$$\sigma_s = \sqrt{8\rho_0 \epsilon_r \epsilon_0 k_B T} \cdot \sinh\left(\frac{ze\Phi_0}{2k_B T} \right), \tag{4}$$

where ρ_0 is the ionic concentration, z is the valency of the salt used and Φ_0 is the surface potential. The temperature is represented by T and k_B is the Boltzmann constant.

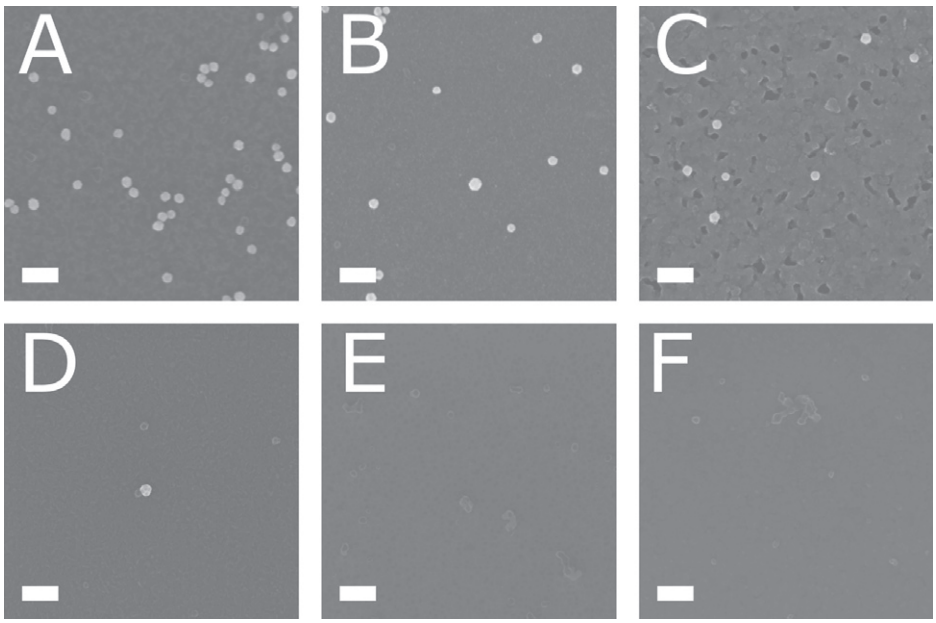

Fig. 2: SEM zoom ins of the six different regions. A: Al; B: Ni; C: Cu; D: V; E: Si/SiO_2; F: Au. The scale bar is 200 nm.

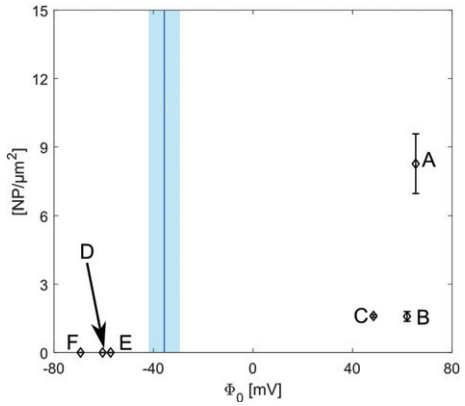

Fig. 3: (Colour online) Upper image; NP densities on six different materials (Au, V, SiO_2, Cu, Ni and Al) plotted against the surface potential measured from AFM. The blue line represents the mean zeta-potential (−35.96 mV) measurement of the NP dispersion and the blue area the zeta-potential standard deviation (±10.9 mV).

Results and discussion. – An example SEM overview of the hexagonal pattern created with the laser writer can be seen in the insert of fig. 1. Each surface is marked in order to easily distinguish between the fields. Each Si/SiO_2 chip is equipped with 16 hexagonal structures. TEM investigations showed that the particles had an average size of 60 nm with a standard error of ±6.2 nm.

Examples of magnified SEM micrographs in each domain after deposition of NPs can be seen in fig. 2A–F. A corresponds to Al, B to Ni, C to Cu, D to V, E to SiO_2 and F to Au. The highest density was found on Al, Ni and Cu that had almost the same density. The density on V, SiO_2 and Au was zero, except for one or two particles in total, these particles are believed to be there due to contaminations present on the surface.

The NP densities *vs.* the surface potential of each material, calculated from 10 image samples with a size of $12\,\mu m \times 8\,\mu m$ and between 0 and 800 NPs in each image, can be seen in fig. 3. The blue line present in the image indicates the zeta potential of the NP dispersion, measured to −35.96 mV and the light blue area represents the standard error measured to ±10.9 mV. The sign from the surface charge density measurements, performed with the AFM, could not be extracted and was therefore assumed to be negative for SiO_2, V and Au and positive for Al, Ni and Cu. The reason for this is because the IEP for V_2O_5, SiO_2, Au [36–38], is lower than the *p*H of the NP dispersion [18]. The tabulated values for IEP as well as the surface potentials and NP densities can be seen in table 1, the standard errors are presented in parenthesis. The surface charge density is obtained by fitting eq. (1) to AFM force curves. The surface charge density is then derived from eq. (4). The surface potential is the surface potential between the surface and the bulk solution.

One can see from the plot in fig. 3 that it is expected that there are no NP found in F, D and E since these surfaces have almost the double negative surface charge compared to the zeta potential of the NPs. It is also expected that NPs are found on C, B and A since the surface charge is positive. The highest NP density was found on Al, which also has the highest surface potential. Al_2O_3 naturally forms on Al, creating a uniform oxide layer which could, in addition to the high surface potential, explain the high NP density. It should be noted that factors such as surface morphology and contaminations could affect the deposition of the NPs as well. The AFM measurements are also performed on monovalent ions, a more

Table 1: IEP [36–38], surface potential and NP density on the different surfaces.

Sample	A	B	C	D	E	F
Φ_0 (mV)	65.4 (±0.4)	61.9 (±0.2)	48.4 (±1.0)	−60.5 (±0.2)	−57.3 (±0.4)	−69.3 (±0.3)
density (NP/μm^2)	8.3 (±1.3)	1.6 (±0.2)	1.6 (±0.06)	0	0	0
IEP	8,7	12	9.5	1.4	3.9	5.2

precise measurement could be achieved by using a trivalent:monovalent ions mixture.

One could expect that Ni should have the highest surface potential, hence also the highest density of NPs; when compared with the IEP for the different metals, the IEP for Al_2O_3 is lower compared to that of NiO. However, this is not the case, Al has a higher surface potential, which is confirmed by the high number of NPs found on that surface. This means that IEP is perhaps not the most exact way of predicting the surface potential of different materials.

Conclusion. – In this work, we have deposited citrate stabilized gold NPs for 1 h on microstructures, made by laser lithography, consisting of six different surfaces (V, SiO_2, Au, Al, Cu and Ni). The NP density was analyzed using an image processing software. The surface potential for each material was calculated from the surface charge density measured *in situ*, in water by an AFM. It was found that no particle sticks on V, SiO_2 or Au. On the other hand particles were found on both Cu, Ni and Al. The zeta potential of the NP dispersion was measured to −35 mV, hence was repelled from a surface more negative than −35 mV and attracted to a surface more positive than −35 mV. The highest NP density was found on the Al surfaces, which also had the highest surface potential (65.38 mV). Constant development of this kind of research is important in order to get better understanding of parameters that are involved in the deposition of colloidal NPs on surfaces (zeta and surface potential). This, in turn, allows for application in a broad range of areas such as targeting drugs and plasmonic sensing. Guidance of NPs is in particular interesting regarding single molecular electronics, where NPs can act as platform for anchoring molecules [12]. It is envisioned that particles can then be guided to specific sites, of different metals, on a prefabricated substrate and in the end build up a logic circuit [11,39]. This work has shown that the IEP may not the best way of predicting the surface potential in water for different materials and it is therefore important to continue research with mapping the surface potential of different materials in order to be able to advance within colloidal science. One can see that the number of particles depends on the surface potential and that an increased potential results in an increased number of NPs. However, other factors such as surface contamination in the deposition, morphology of the surface, and change of surface charge as it accumulates particles are not treated in this work and need to be addressed in future research.

* * *

This work was supported by the Myfab National Access program (at MC2 Nano Fabrication Laboratory, Chalmers), the Knut and Alice Wallenberg Foundation, Chalmers Area of Advance Nano, NanoGeoScience group at UCPH and the European Research Council through ERC StG SIMONE.

REFERENCES

[1] Gulson B., Mccall M., Korsch M., Gomez L., Casey P., Oytam Y., Taylor A., Mcculloch M., Trotter J., Kinsley L. and Greenoak G., *Toxicol. Sci.*, **118** (2010) 140.

[2] Reed R. B., Zaikova T., Barber A., Simonich M., Lankone R., Marco M., Hristovski K., Herckes P., Passantino L., Fairbrother D. H., Tanguay R., Ranville J. F., Hutchison J. E. and Westerho P. K., *Environ. Sci. Technol.*, **50** (2016) 4018.

[3] Kim T., Fu X., Warther D. and Sailor M. J., *ACS Nano*, **11** (2017) 2773.

[4] Zhang Z.-c., Xu B. and Wang X., *Chem. Soc. Rev.*, **43** (2014) 7870.

[5] Haley B. and Frenkel E., *Urol. Oncol.*, **26** (2008) 57.

[6] Fouad R. R., Aljohani H. A. and Shoueir K. R., *Mar. Pollut. Bull.*, **112** (2016) 46.

[7] Gschneidtner T. A., Fernandez Y. A. D., Syrenova S., Westerlund F., Langhammer C. and Moth-Poulsen K., *Langmuir*, **30** (2014) 3041.

[8] Borglin J., Guldbrand S., Evenbratt H., Kirejev V., Grönbeck H. and Ericson M. B., *Appl. Phys. Lett.*, **107** (2015) 234101.

[9] Lundgren A., Hulander M., Brorsson J., Hermansson M., Elwing H., Andersson O., Liedberg B. and Berglin M., *Part. Part. Syst. Charact.*, **31** (2014) 209.

[10] Manheller M., Karthäuser S., Waser R., Blech K. and Simon U., *J. Phys. Chem. C*, **116** (2012) 20657.

[11] Fernandez Y. A. D., Gschneidtner T. A., Wadell C., Fornander L. H., Lara-Avila S., Langhammer C., Moth-Poulsen K. and Westerlund F., *Nanoscale*, **6** (2014) 14605.

[12] Dadosh T., Gordin Y., Krahne R., Khivrich I., Mahalu D., Frydman V., Sperling J., Yacoby A. and Bar-Joseph I., *Nature*, **436** (2005) 677.

[13] Gschneidtner T. A., Diaz Fernandez Y. A. and Moth-Poulsen K., *J. Mater. Chem. C*, **1** (2013) 7127.

[14] Ruffino F., Canino A., Grimaldi M. G., Giannazzo F., Bongiorno C., Roccaforte F. and Raineri V., *J. Appl. Phys.*, **101** (2007) 064306.

[15] Dick K., *Epitaxial growth and design of nanowires and complex nanostructures*, PhD Thesis, Lund University (2007).
[16] Mielke J., Dohányosová P., López S. and Hodoroaba V.-D., *Microsc. Microanal.*, **22** (2016) 1846.
[17] Tsai D.-H., Kim S. H., Corrigan T. D., Phaneuf R. J. and Zachariah M. R., *Nanotechnology*, **16** (2005) 1856.
[18] Eklöf J., Gschneidtner T., Lara-Avila S., Nygård K. and Moth-Poulsen K., *RSC Adv.*, **6** (2016) 104246.
[19] Rey A., Billardon G., Lortscher E., Moth-Poulsen K., Stuhr-Hansen N., Wolf H., Bjørnholm T., Stemmer A. and Riel H., *Nanoscale*, **5** (2013) 8680.
[20] Ni S., Klein M. J. K., Spencer N. D. and Wolf H., *Langmuir*, **30** (2014) 90.
[21] Moth-Poulsen K., Kofod-Hansen V., Kamounah F. S., Hatzakis N. S., Stamou D., Schaumburg K. and Christensen J. B., *Bioconj. Chem.*, **21** (2010) 1056.
[22] Gu Y.-J., Cheng J., Lin C.-C., Lam Y. W., Cheng S. H. and Wong W.-T., *Toxicol. Appl. Pharmacol.*, **237** (2009) 196.
[23] Celler G. and Trimble L., *Appl. Surf. Sci.*, **39** (1989) 245.
[24] Smallman R. and Ngan A., *Physical Metallurgy and Advanced Materials Engineering* (Butterworth-Heinemann, Oxford) 2007.
[25] Su Q., Huang C., Wang Y., Fan Y., Lu B., Lan W., Wang Y. and Liu X., *J. Alloys Compd.*, **475** (2009) 518.
[26] Lee S.-K., Hsu H.-C. and Tuan W.-H., *Mater. Res.*, **19** (2016) 51.
[27] Lambers E. S., Dykstal C. N., Seo J. M., Rowe J. E. and Holloway P. H., *Oxid. Met.*, **45** (1996) 301.
[28] Kosmulski M., *Chemical Properties of Material Surfaces* (Marcel Dekker, Inc., New York) 2001.
[29] Kosmulski M., *Surface Charging and Points of Zero Charge* (CRC Press Taylor and Francis Group) 2009.
[30] Israelachvili J. N., *Intermolecular and Surface Forces*, 3rd edition (Academic Press, San Diego) 2011.
[31] Butt Hans-Jürgen, Graf Karlheinz and Kappl Michael, *Physics and Chemistry of Interfaces* (Wiley-VCH-Verlag, Weinheim) 2013.
[32] Drelich J., Long J. and Yeung A., *Can. J. Chem. Eng.*, **85** (2007) 625.
[33] Yin X. and Drelich J., *Langmuir*, **24** (2008) 8013.
[34] Zhao C., Ebeling D., Siretanu I., van den Ende D. and Mugele F., *Nanoscale*, **7** (2015) 16298.
[35] Shi L., Olsson M. H. M., Hassenkam T. and Stipp S. L. S., *Energy Fuels*, **30** (2016) 5346.
[36] Gil-Llambías F. J., Escudey A. M., Fierro J. L. G. and Agudo A. L., *J. Catal.*, **95** (1985) 520.
[37] Cuddy M. F., Poda A. R. and Brantley L. N., *ACS Appl. Mater. Interfaces*, **5** (2013) 3514.
[38] Kittaka S. and Morimoto T., *J. Colloid Interface Sci.*, **75** (1980) 398.
[39] Jain T., Tang Q., Bjørnholm T. and Nørgaard K., *Acc. Chem. Res.*, **47** (2014) 2.